Superlattices and Microstructures 45 (2009) 435–443

Contents lists available at ScienceDirect

Superlattices and Microstructures

journal homepage: www.elsevier.com/locate/superlattices

Electrical properties of pinholes in GaN:Mn epitaxial films characterized by conductive AFM

M. Herrera [a,1], A. Cremades [a,*], M. Stutzmann [b], J. Piqueras [a]

[a] Departamento de Física de Materiales, Facultad de Ciencias Físicas, Universidad Complutense de Madrid, Madrid 28040, Spain
[b] Walter Schottky Institute, Technical University Munich, Am Coulombwall, D-85748 Garching, Germany

ARTICLE INFO

Article history:
Available online 8 January 2009

Keywords:
GaN
Leakage current
AFM
Manganese doping
Cathodoluminescence

ABSTRACT

Mn doped GaN films have been studied by conductive Atomic Force Microscopy (AFM), Cathodoluminescence (CL) and Electron Beam Induced Current (EBIC). AFM measurements revealed the presence of pinholes with diameters between 130 and 380 nm. The distribution, density and size of the pinholes depend on the Mn doping concentration. AFM Leakage Current images (LC) show a defined contrast at the pinhole planes $\{101\bar{1}\}$ in the sample with Mn concentration of 6.2×10^{20} cm^{-3}. For the sample with an Mn concentration of 1.1×10^{20} cm^{-3}, LC contrast appears around the pinholes, while no LC contrast was observed for sample with lower Mn concentration. CL measurements indicate that the samples exhibit strain related to Mn incorporation. In correlation with LC measurements, EBIC images show that pinholes are recombination sites. The combination of these techniques enabled us to analyze the Frenkel–Poole conduction in the samples and its relationship with the residual strain and the doping concentration in the films, which would exclude the mechanism of conduction through dislocations.

1. Introduction

Threading dislocations with a screw component are the origin of high leakage currents in devices based on nitride semiconductors. A number of articles [1–4] report conductive AFM as a tool to

* Corresponding author. Tel.: +34 913944521.
E-mail address: cremades@fis.ucm.es (A. Cremades).
[1] Permanent address: Centro de Nanociencias y Nanotecnología, UNAM Km. 107 Carretera Tijuana-Ensenada, Apdo. Postal 356, Ensenada 22800, B.C., Mexico.

0749-6036/$ – see front matter © 2008 Elsevier Ltd. All rights reserved.
doi:10.1016/j.spmi.2008.12.023

Table 1
Mn content and resistivity of GaN samples prepared by PI-MBE.

Sample no.	Mn (cm^{-3})	Resistivity (Ω cm)
1	6.2×10^{20}	17.2×10^{-3}
2	1.1×10^{20}	46.7
3	5.3×10^{19}	2.5×10^{7}

image the current paths of these structures. By simultaneously mapping topography and current distribution, C-AFM allows us to establish a direct correlation of the contacted area with its electrical properties, which makes this technique very useful to identify and investigate localized current paths. However, in previous works the recorded AFM images are usually more than 5 μm wide, while atomic force microscopy typically resolves nanometric structures. As a result the details of conduction through the dislocation area are ignored and the general assumption of conductivity associated to dislocations is assumed. Several studies for both, metalorganic chemical-vapor deposited (MOCVD) [5] GaN films as well as for GaN grown by molecular-beam epitaxy (MBE) [6] have shown that conduction along threading dislocations (TD) is the primary mechanism responsible for the leakage current in the films. In Ref. [5], films with a high density of TD dislocation and almost dislocation free epitaxial lateral overgrowth films were compared, concluding that reverse-bias leakage current is strongly influenced by the TD density. The results reported in Ref. [6] show that in similarly grown material most of the current leakage paths are located on spiral hillocks, suggesting that screw or mixed dislocations are responsible for the leakage current. On the contrary, other works show that not all the dislocations with screw component conduct current or have an influence on the detected leakage current [4,7]. The previous results indicate that the electrical behavior of dislocations is significantly influenced by the growth conditions.

The objective of this work is to study the role of threading dislocations and defects in the conduction mechanism exhibited by GaN films doped with Manganese. In this work Mn doped GaN films have been studied by conductive AFM, CL and EBIC in the the scanning electron microscope. The combination of these techniques allows us to analyze the Frenkel–Poole conduction exhibited by the samples and its relation with the residual strain and the doping concentration in the films.

2. Experimental setup

The Mn doped GaN films were grown on (0001) sapphire by Plasma Induced Molecular Beam Epitaxy (PI-MBE). The samples were grown in Ga-rich conditions, with a growth window for the Ga flux around $p(\mathrm{Ga}) = 2 \times 10^{15}$ cm^{-2} s^{-1}. The Nitrogen flux was held constant for all the samples $p(\mathrm{N}) = 8 \times 10^{14}$ cm^{-2} s^{-1}. With these conditions a better incorporation of nitrogen into the lattice was induced, and high crystalline quality was obtained. Due to the growth under metal-rich conditions, metallic droplets were formed at the film surface. The droplets were removed by HCl etching. A detailed description of the growth procedure can be found in Ref. [8]. The samples consist of a 10 nm-thick AlN buffer layer on a sapphire substrate and a 1.2 μm-thick Mn doped GaN epilayer. Three samples with different impurity concentrations were prepared. The impurity concentration was recorded by elastic recoil detection (ERDA) (Table 1). Sheet resistivity measurements by the van der Pauw method at room temperature were obtained by four small electrical contacts fabricated with silver paint, using a Keithley 2400 as power supply and amperemeter. The resistivity values of the samples are shown in Table 1.

The films were studied by Atomic Force Microscopy (AFM) in Conducting-AFM (C-AFM) mode using a Nanotec-SPM operated at room temperature. For C-AFM experiments, forward leakage current (LC) was measured by applying a voltage bias between a conductive cantilever covered with Pt–Cr and a contact fabricated with Ag paint on the sample. In our setup, the sample is polarized and the cantilever tip is grounded. Forward current corresponds to a positive voltage applied to the sample. The leakage current collected through the Schottky contact formed between cantilever and GaN surface was detected using a Keithley-428 current amplifier. The electrical properties of the samples were also studied by Electron Beam Induced Current (EBIC) and Cathodoluminescence (CL)

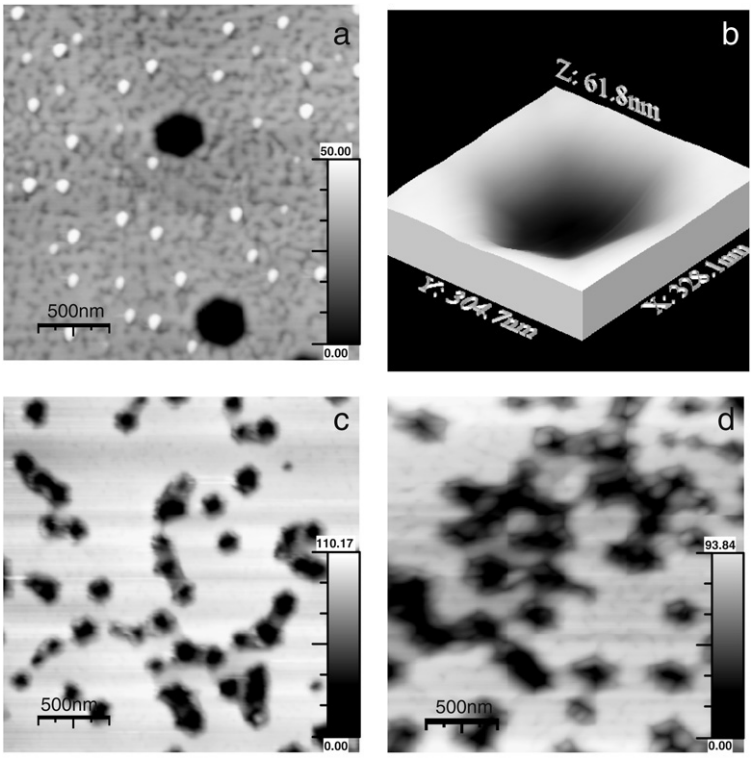

Fig. 1. (a) AFM images of sample 1 with several metallic Mn dots and (b) 3D image of V-shaped pinhole, and of (c) samples 2 and (d) sample 3 with grouped pinholes.

in the scanning electron microscopy. A Leica S-440 scanning electron microscope with electron beam energies between 10 and 15 keV was used. For EBIC measurements Au/GaN Schottky contacts were used in planar configuration. CL measurements were performed at a sample temperature of 77 K in the visible range with a Hamamatsu R928 photomultiplier and a Hamamatsu PMA-11 CCD camera. An Oriel computer controlled monochromator was used for spectral analysis of the emission.

3. Results

AFM topographical measurements revealed the formation of pinholes with diameters between 130 and 380 nm (Fig. 1) in the samples. The AFM images of sample 1 with the highest content of Mn, show isolated pinholes with diameters of about 300 nm in a surface composed of numerous pits and droplets of residual metallic Mn (Fig. 1(a)). 3D Normal-force images acquired in this sample revealed the typical V shape of pinholes formed by the $\{10\bar{1}1\}$ pyramidal planes [9,10] (Fig. 1(b)). The average density of pinholes in sample 1, measured from the AFM images was about 3×10^7 cm^{-2}. Pinholes were also found in samples 2 and 3 (Fig. 1(c) and (d)) with an average diameter of about 150 and 270 nm, respectively. The density of pinholes varies from 9×10^8 cm^{-2} for sample 2 with the smallest pinholes to 7×10^8 cm^{-2} for sample 3. The pinholes in samples 2 and 3 usually form groups of several pinholes sharing a common hollow area on the surface as observed in Fig. 1(b) and (c). The RMS roughness of the film surface decreased with the incorporation of manganese in the final film composition. Typical values obtained from AFM images are about 0.7 nm for sample 1, 8.7 nm for sample 2, and 12.6 nm for sample 3.

LC images of sample 1 recorded on the region shown in Fig. 2(a), show contrast at the oblique pinhole planes for a forward bias higher than 1 V (Fig. 2(b) and (c)). For other regions far from pinholes,

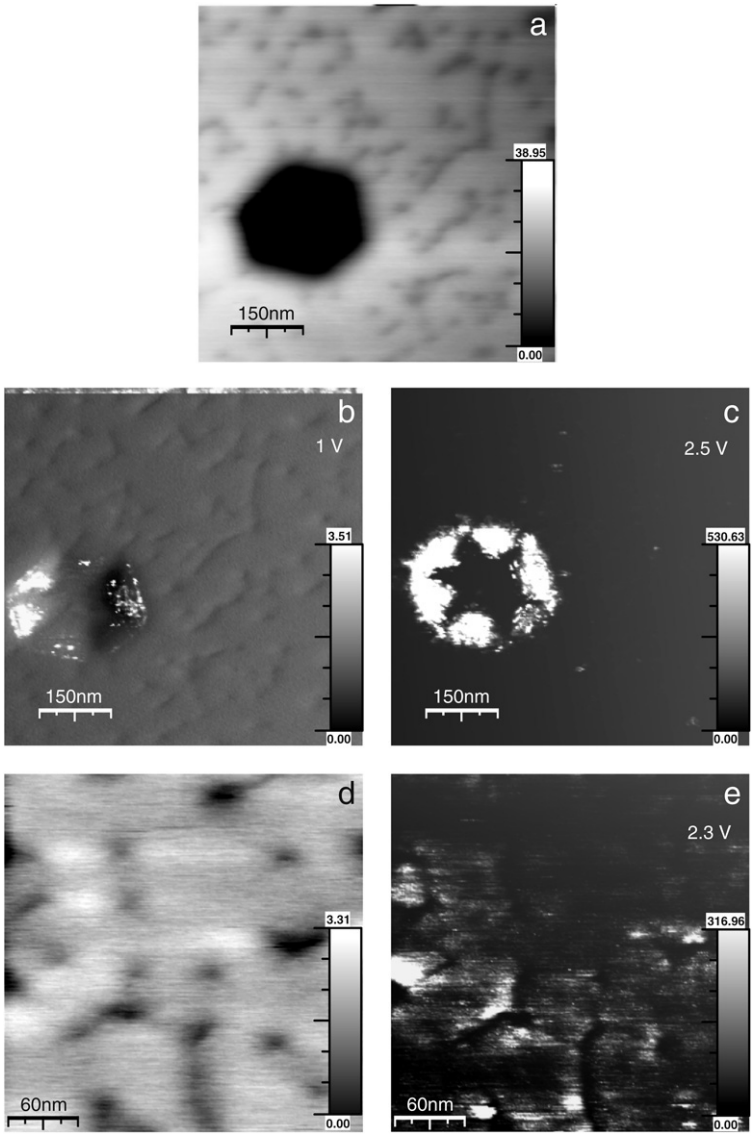

Fig. 2. (a) AFM and (b) and (c) C-AFM images of a pinhole in sample 1 with electrical activity at 1 V and 2.5 V, and (d) the surface of this sample with (e) leakage current signal at 2.3 V. Z-scale in C-AFM images is giving in pA.

as the one shown in Fig. 2(d), the LC images show a contrast with bright regions and dark lines which seems to be related to the grain structure of the film (Fig. 2(e)). The surface of sample 2, as the area shown in Fig. 3(a) and (b), exhibits LC contrast (Fig. 3(c)). As observed in Fig. 3(d) by superimposing the topographic and C-AFM images, the contrast is related to the surrounding areas of the pinhole groups. For sample 3 no LC signal was detected.

Representative I–V curves of different regions in samples 1 and 2 (Fig. 4(a)), show that detectable forward LC is produced for an applied bias higher than 1.5 V in sample 1 and 3.5 V in sample 2. These measurements show a linear relation between ln (I) and the square root of the applied voltage $\sqrt{V}$ (Fig. 4(b)), which indicates Frenkel–Poole conduction in the samples. I–V curves acquired in a pinhole

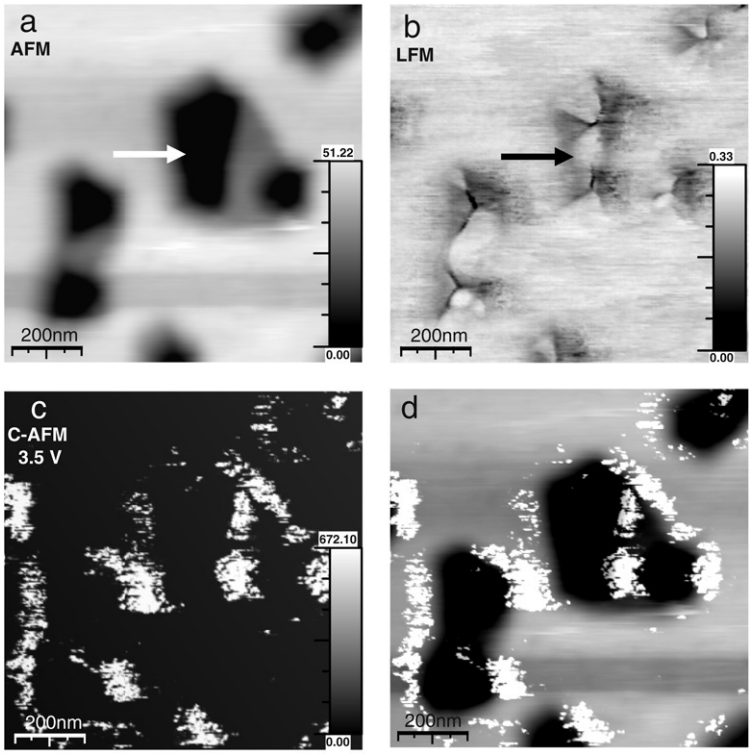

Fig. 3. (a) AFM image and (b) lateral-force-AFM image (z-scale in nN) of pinholes in sample 2. (c) C-AFM image of this region recorded at 3.5 V with a leakage current produced around the pinhole (z-scale in pA), as the composed image (d) shows.

of sample 1 revealed LC signal by forward and reverse bias (Fig. 4(c)), with a hysteresis produced with the change in direction of the applied voltage ramp. To acquire an I/V curve, our AFM system first applies a forward bias during 168 ms, and then a reverse bias for 168 ms. Fig. 4(b) and (d) were plotted from forward bias (from negative to positive voltages). This behavior was observed at long separations between the cantilever and the Ag paint contact, and can be associated to the slow electric response of the defect with the variation of the applied bias voltage, although the conduction mechanism is also of Frenkel–Poole type as shown in Fig. 4(d).

Fig. 5 shows EBIC images that reveal a decrease of the collected current at pinholes, which appear as small dark spots of about 200 nm in diameter. Similar types of dots are observed in EBIC images of Si doped AlGaN films [11].

CL spectra were acquired at 15 kV. High (low) excitation density corresponds to a beam-current density of about 7.8×10^{-5} nA/μm^2 (1.9×10^{-7} nA/μm^2). CL spectra of an extended area of the samples 1 and 2, acquired at high excitation density show a band centered at about 3.49 eV with a shoulder centered at about of 3.4 eV (Fig. 6(a)), which correspond to band edge and defect related emissions. The sample 3 exhibits a broad emission centered at about 3.37 eV. CL spectra acquired with low density of excitation show bands centered at 3.35, 3.33 and 3.25 eV for samples 1, 2 and 3 respectively (Fig. 6(b)). Deconvolution of the CL spectra of samples 1 and 2 (not presented here) shows two components centered at about 3.35 and 3.0 eV.

4. Discussion

As described above, the density of V-defects, between 10^7 and 10^8 cm^{-2}, in the Mn doped GaN films, corresponds to the expected dislocation density in this kind of samples. TEM studies of

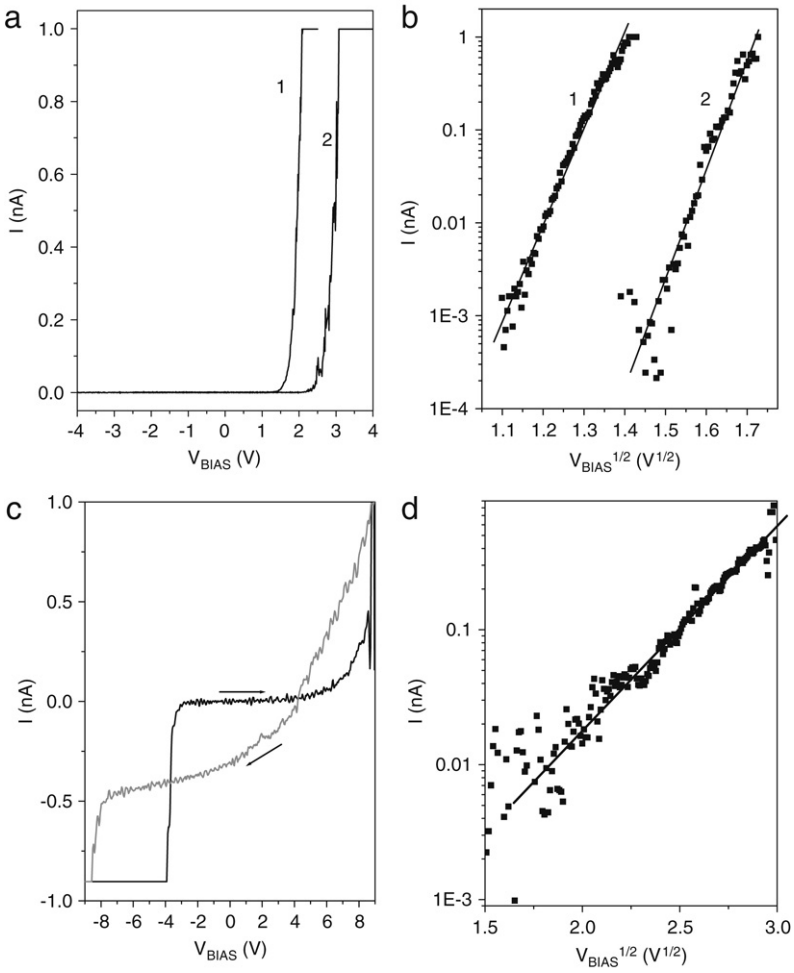

Fig. 4. (a) Leakage current values recorded by forward bias applied in samples 1 and 2. (b) The plot of current and bias square root reveals a Frenkel–Poole conduction mechanism in samples. (c–d) Leakage current signal recorded in a pinhole of sample 1 revealed the same conduction mechanism.

V-pinholes in GaN films have shown that dislocations and inversion domains in GaN are responsible for the formation of V-defects [9,12,13]. However, in the growth of GaN on AlN as buffer film by MOCVD, these defects are formed at the interface GaN/AlN by chemical etching around the threading dislocations of the AlN film [12]. The angle between the arms of V-defects measured in AFM images is between 50° and 60°, which agrees with the value of 56° expected to the $\{10\bar{1}1\}$ planes in GaN. From this angle, and the diameter of the V-pinholes, the depth range of these defects was estimated to be between 44 and 128 nm. The depth of the pinholes measured directly from the AFM Z-profile agrees with these values, although these measurements could underestimate the actual depth values, depending on the ratio between the tip diameter and the pinhole diameter near the pinhole apex. Since the GaN film has a thickness of 1200 nm it appears that the V-pinholes are not formed at the GaN/AlN interface. As the pinholes are not formed at the interface, threading dislocations or misfit are excluded to induce pinhole formation. Therefore, pinhole formation should be related to the residual stress in the films induced by doping with Mn. Moreover, similar defects have been found also in

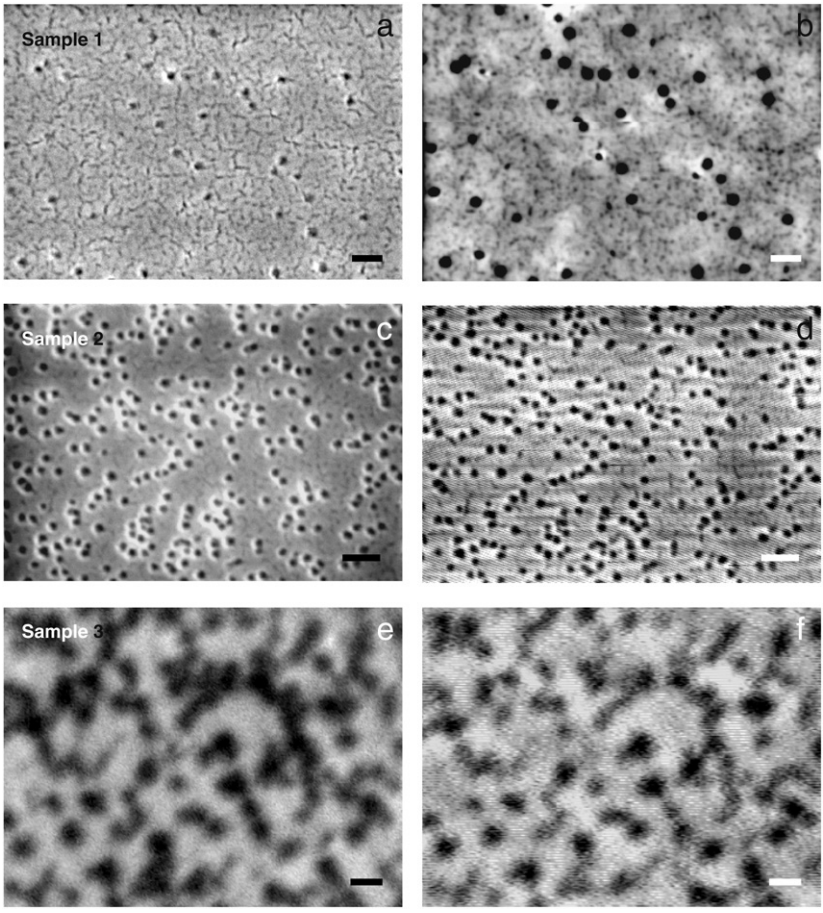

Fig. 5. (a), (b) and (e) SEM and (b), (d) and (f) EBIC images of samples with pinholes recorded as black spots. The bar in the figures corresponds to 300 nm.

InGaN [14] and AlInGaN [10] thin films and their formation has been attributed to the residual strain in the films [15].

C-AFM measurements revealed forward and reverse leakage current from pinholes in sample 1, which follows a Frenkel–Poole current–voltage characteristics (Fig. 4). Within this model, the current is produced by a field-assisted thermal activation of electrons located in deep levels [16]. Conductivity associated with dislocations is a common assumption when the origin of the leakage current in different semiconductors is analyzed. For GaN and AlGaN samples, Zhang et al. [1] concluded from the analysis of temperature-dependent current–voltage characteristics measured in a Conductive AFM system, that at room temperature the current flow is due to the emission of electrons from a trap state near the metal–semiconductor interface into a continuum of states associated with each conductive dislocation. Although deep acceptors and electric charge at threading dislocations in GaN are expected [17,18], the LC signal in the samples occur very far from the center of V-defects (more that 50 nm), so that the leakage current at the pinholes cannot be related directly to the presence of a dislocation whose core is located at the apex of the pinhole, but rather to the distribution of defects and impurities in this area due to the stress relaxation induced by the pinhole formation. Strain in Mn doped GaN films possibly can explain the origin of the deep defects responsible for the LC signal. Due to the lattice and the thermal expansion coefficient mismatches between the GaN films and the sapphire

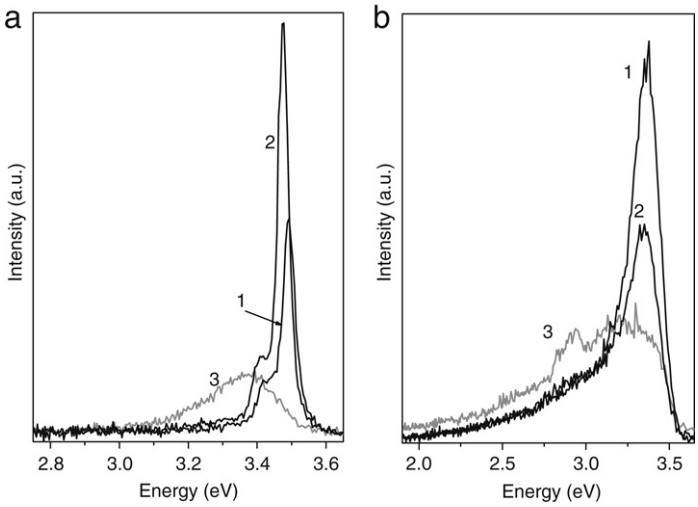

Fig. 6. CL spectra of samples recorded for (a) high and (b) low electron excitation conditions.

substrate these samples exhibit biaxial strain. Another origin of the strain is the incorporation of a high amount of Mn [19]. Therefore, the current should be produced by the emission of electrons from traps or deep levels introduced by defects or impurities, which are present in the $\{10\bar{1}1\}$ planes, directly into the semiconductor. Also, we have previously found recombination of carriers at dislocations through a shallow acceptor level located at about 20 meV above the valence band for AlGaN [11], a mechanism that is in competition with a conduction process.

In sample 2, an LC-signal was recorded only around V-defects as shown in Fig. 3(c). Any drift of both images (topographic and current images) can be excluded as they are recorded simultaneously. For this sample with lower doping concentration, the strain distribution around the pinholes should differ significantly from that of sample 1, as not only the size but also the pinhole distribution is totally different for both samples as reported in the results section. The relaxed areas are probably located around the groups of pinholes similarly to the studied strain distribution in pinholes of InGaN films [14]. There, an accumulation of Indium around the pinhole due to the relaxed strain in this area was reported.

The low conductance of the sample 3 is explained by the pinning of the Fermi level by surface states [20], resulting in the formation of a surface depletion layer which extend in thickness due to the low doping concentration of the film. This depletion layer is located under the nanoscale Schottky diode formed at the contact region between the metal tip and the film surface.

The luminescence of the samples is often affected by the residual strain in the films. A shift in the energy of the near band gap luminescence peak is commonly observed due to the variation in the value of the band gap induced by the lattice strain. This trend is observed in the CL spectra of Fig. 6. In samples with higher Mn content the near band gap luminescence is shifted to higher energies. The observed blue shift of the GaN near band edge is produced by the strong compressive strain generated by the high concentration of Mn in the films, as previously reported [21]. The intensity and width of the bands are also reduced and increased, respectively, in strained samples mainly due to a reduction in the crystal quality. In our case the samples which exhibit less luminescence intensity are those with Mn concentrations below 10^{20} cm^{-3}. The incorporation of Mn concentration seems to improve the crystal quality probably due to some degree of clustering. The yellow emission band related to Ga vacancies is not present in our CL spectra. This is an indication of the incorporation of Mn to the Ga sublattice, similarly to the effect of Mg doping of GaN. No intraionic emissions of Mn could be detected between 500 nm (2.48 eV) and 900 nm (1.37 eV). Although the samples are Mn doped they exhibit *n*-conduction due to the fact that the Mn creates a deep acceptor, which is difficult to ionize. From

electron spin resonance Mn is known to be mainly present in the neutral acceptor state (Mn^{3+}) in GaN without codoping, localized at 1.8 eV above the valence band edge of GaN [19].

The carrier recombination at the pinholes of the GaN:Mn samples was confirmed by EBIC measurements. The EBIC images reveal a decrease of the collected current at pinholes, which appear as small dark spots of about 200 nm in diameter. Similar types of dots were observed in EBIC images of Si doped AlGaN films [11]. The pinholes of GaN:Mn films exhibit the same behavior at high beam current conditions than the ones in AlGaN, increasing the diameter up to 1 μm and a density of 10^6 cm^{-2}.

5. Conclusions

Manganese doped GaN films have been characterized by conductive AFM, CL and EBIC. The incorporation of manganese influences the conductivity of the samples, as well as the pinhole formation and density. The observed leakage current is related to the areas close to pinholes and exhibits a Frenkel–Poole conduction mechanism. The observed leakage current at the pinholes cannot be related directly to the presence of a dislocation whose core is located at the apex of the pinhole, but rather to the distribution of defects and impurities in this area due to the stress relaxation induced by the pinhole formation. Strain in Mn doped GaN films possibly explains the origin of the deep defects responsible for the LC signal.

Acknowledgement

This work was supported by MEC (Project MAT2006-01259).

References

[1] H. Zhang, E.J. Miller, E.T. Yua, J. Appl. Phys. 99 (2006) 023703.
[2] H. Zhang, E.T. Yua, J. Appl. Phys. 99 (2006) 014501.
[3] E.J. Miller, D.M. Schaadt, E.T. Yua, P. Waltereit, C. Poblenz, J.S. Speck, Appl. Phys. Lett. 82 (2003) 1293.
[4] E.J. Miller, D.M. Schaadt, E.T. Yu, C. Poblenz, C. Elsass, J.S. Speck, J. Appl. Phys. 91 (2002) 9821.
[5] P. Kozodoy, J.P. Ibbetson, H. Marchand, P.T. Fini, S. Keller, J.S. Speck, S.P. DenBaars, U.K. Mishra, Appl. Phys. Lett. 73 (1998) 975.
[6] J.W.P. Hsu, M.J. Manfra, D.V. Lang, S. Richter, S.N.G. Chu, A.M. Sergent, R.N. Kleiman, L.N. Pfeiffer, R.J. Molnar, Appl. Phys. Lett. 78 (2001) 1685.
[7] K. Shiojima, T. Suemitsu, M. Ogura, Appl. Phys. Lett. 78 (2001) 3636.
[8] T. Graf, M. Gjukic, M. Hermann, M.S. Brandt, M. Stutzmann, L. Görgens, J.B. Philipp, O. Ambacher, J. Appl. Phys. 93 (2003) 9697.
[9] Z. Liliental-Weber, Y. Chen, S. Ruvimov, J. Washburn, Phys. Rev. Lett. 79 (1997) 2835.
[10] M. Herrera, A. Cremades, J. Piqueras, M. Stutzmann, O. Ambacher, J. Appl. Phys. 95 (2004) 5305.
[11] M. Albrecht, A. Cremades, J. Krinke, S. Christiansen, O. Ambacher, J. Piqueras, H.P. Strunk, M. Stutzmann, Phys. Status Solidi (B) 216 (1999) 409.
[12] J. Bai, T. Wang, P.J. Parbrook, I.M. Ross, J. Cullis, Cryst. Growth 289 (2006) 63.
[13] K.S. Son, D.G. Kim, H.K. Cho, K. Lee, S. Kim, K. Park, J. Cryst. Growth 261 (2004) 50.
[14] A. Cremades, M. Albrecht, J.M. Ulloa, J. Piqueras, H.P. Strunk, D. Hanser, R.F. Davis, Mat. Res. Soc. Proc. 588 (2000) 81–86.
[15] M. Shiojiri, C.C. Chuo, J.T. Hsu, J.R. Yang, H. Saijo, J. Appl. Phys. 99 (2006) 73505.
[16] S.D. Ganichev, E. Ziemann, W. Prettl, I.N. Yassievich, A.A. Istratov, E.R. Weber, Phys. Rev. B 61 (2000) 10361.
[17] J. Elsner, R. Jones, M.I. Heggie, P.K. Sitch, M. Haugk, Th. Frauenheim, S. Öberg, P.R. Briddon, Phys. Rev. B 58 (1998) 12571.
[18] D. Cherns, C.G. Jiao, Phys. Rev. Lett. 87 (2001) 205504.
[19] T. Graf, M. Gjukic, M. Hermann, M.S. Brandt, M. Stutzmann, O. Ambacher, Phys. Rev. B 67 (2003) 165215.
[20] I. Tanaka, I. Kamiya, H. Sakaki, N. Qureshi, S.J. Allen Jr., P.M. Petroff, Appl. Phys. Lett. 74 (1999) 844.
[21] O. Gelhausen, E. Malguth, M.R. Phillips, E.M. Goldys, M. Strassburg, A. Hoffmann, T. Graf, M. Gjukic, M. Stutzmann, Appl. Phys. Lett. 84 (2004) 31.